Inorganic Chemistry Communications 119 (2020) 108085

Contents lists available at ScienceDirect

Inorganic Chemistry Communications

journal homepage: www.elsevier.com/locate/inoche

Short communication

Highly selective and potent anti-cancer agents based on 2,9-substituted-1, 10-phenanthroline derivatives

Sourav De, S.K. Ashok Kumar*

Department of Chemistry, School of Advanced Sciences, Vellore Institute of Technology, Vellore 632014, Tamil Nadu, India

GRAPHICAL ABSTRACT

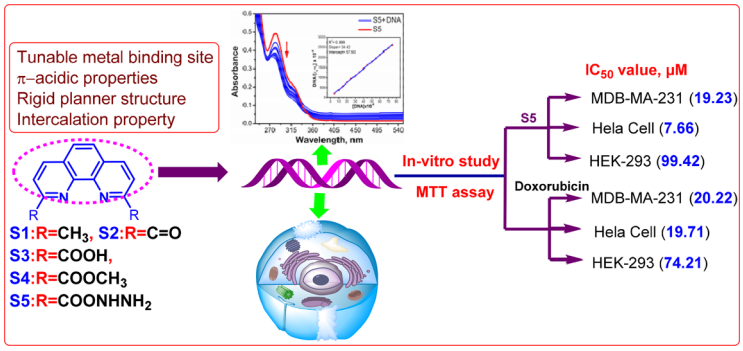

ARTICLE INFO

Keywords:
DNA and BSA binding
Gel electrophoresis
Cytotoxicity study
Molecular docking and DFT

ABSTRACT

A study concerning on *in-vitro* anticancer evaluation of structurally tuned 1,10-phenanthroline at 2,9 positions with different functional groups such as $-CH_3$ (**S1**), > C═O (**S2**), –COOH (**S3**), $-COOCH_3$ (**S4**) and $-CONHNH_2$ (**S5**) were described. The solubility data revealed that all ligands were completely soluble in dimethyl sulphoxide (DMSO) and moderately soluble in water. The photo-physical properties of these ligands revealed that a common absorption peak appeared in the region of 270–300 nm and emission spectra in the region of 330–510 nm with a large Stokes shift of 85 nm. The binding constant of ligands (**S1**-**S5**) with calf-thymus deoxyribonucleic acid (CT-DNA) and bovine serum albumin (BSA) were found to be $10^5\ M^{-1}$ and $10^4\ M^{-1}$ respectively. The fluorescence quenching of ethidium bromide (EtBr) from DNA upon addition of ligand was confirmed from binding affinity values K_{SV} ($10^4\ M^{-1}$) and K_{app} ($10^6\ M^{-1}$). The mode of interaction of ligand with DNA is either by intercalation or groove binding this is further supported by viscosity and *in-silico* studies. The gel electrophoresis studies exhibited that **S4** and **S5** have cleaved plasmid DNA completely within 60 min while rest of the ligands took more than 60 min. The cytotoxicity study of these ligands (**S1**-**S5**) were conducted with two different cancer cell lines (MDA-MB-231 and HeLa) and their performance were compared with normal HEK-293 cells. The study revealed that ligands **S5** and **S4** were found to be least inhibitory concentration (IC_{50}) and high selectivity factor values of 7.66 μM/12.97 and 13.35 μM/6.19 with respect to HeLa and MDA-MB-231 cell lines while ligands **S1**-**S3** showed high IC_{50} values compare to doxorubicin. However, both **S5** and **S4** ligands have been displayed higher cytotoxicity effect than doxorubicin and least effect on normal cell HEK-293.

* Corresponding author.
E-mail address: ashokkumar.sk@vit.ac.in (S.K. Ashok Kumar).

https://doi.org/10.1016/j.inoche.2020.108085
Received 26 April 2020; Received in revised form 26 June 2020; Accepted 29 June 2020
Available online 02 July 2020

1. Introduction

Despite advances in chemotherapy, cancer is a key problem that continues to struggle in our society. The scientific community is thoroughly studying new strategies of treatment for cancer by developing new drugs. The main approach of designing an antineoplastic agent is to destroy the DNA by various binding mechanisms such as hydrophobic binding, electrostatic binding to the minor groove and intercalation. The intercalation can cause deep modifications in the nucleotide secondary structure, such as lengthening, stiffening and unwinding of the DNA helix with major changes in DNA replication and transcription [1]. The complete extent of their cellular process is vital to balance potent and toxicity, is often not understood. In addition, the use of many anticancer drugs is limited by dose-limiting toxicities as well as the development of drug resistance. So, the novel anticancer agents are constantly being prepared to address these issues.

Among several class of compounds, phenanthroline derivatives are important class of compounds due to their various structural and chemical properties; for example, rigidity, planarity, aromaticity, basicity, and chelating capability, which makes them versatile starting materials in many applications such as, luminescence, metal complexation and biological activities. It is present in alkaloids, sterols, and hormones which makes analogues a fair selection in the generation of characteristic bioactive compounds [2–6]. In addition, metal complexes of these ligands are used in molecular assemblies, DNA splitting, building blocks for preparation of metallo-dendrimers, redox agents and catalysis [7–10]. The capability of 1,10-phenanthroline to interact with nucleic acid base pairs have been clearly explained by using computational and experimental [11,12]. In their studies, both adenine–thymine (AT) and cytosine-guanine (GC) base pairs bind phenanthroline unit *via* hydrogen bonding. Therefore, 2.9 substituted phenanthroline compounds have been reported recently by scientists for cellular applications (Fig. 1). Wang *et al.* have reported the inhibitory effect of (**1**) on neck, head and lung cancer cell growth with IC_{50} in the range of 0.1–0.2 μM [13]. In another report, compounds (**2**–**5**) can effectively induce the formation and stabilization of anti-parallel G-quadruplex structure of human telomeric sequence (AG3(T2AG3)3, HTG22), and significantly inhibit telomerase activity and HeLa cell with IC_{50} values 2.0–2.3 μM) proliferation [14]. Neidle *et al.* have reported that a platinum-phenanthroline square complexes (**6** and **7**) can persuade a high degree of quadruplex DNA stabilization and inhibit telomerase activity having IC_{50} value 3.1 and 8.9 μM) [15]. Komarnicka *et al.* have synthesized copper complex (**8**) showed high activity against PANC-1 cell lines with IC_{50} of 2.65 μM [16]. Ewelina *et al.* have prepared complexes (**9**–**10**) and results revealed lower toxicity to normal human cell line with IC_{50} of 0.57 μM and 1.72 μM than A549 cell with IC_{50} value of 0.29 μM and 0.43 μM. The complex (11) reported to be more toxic to normal cells in comparison to cancer cells studied (A549, HeLa, LoVo, and MCF-7) [17]. Kyziol *et al.* have reported copper(I) complexes (**12** and **13**) induce mitochondrial dysfunctions due to reduction of mitochondrial membrane potential leads to mitochondrial damage and causing apoptotic pathways of cellular death by the activation of caspases with IC_{50} value 6.7 and 7.1 μM [18].

As a part of our ongoing research in development of anti-cancer agents, dipyridophenazine compounds (**14**) showed high cytoselectivity and specificity against HeLa cells with IC_{50} of 9.65 μM [19]. Taking into consideration of activity of phenanthroline derivatives reported in literature, recently we have synthesized phenanthroline dicarbohydrazide derivative (**15**) to synthesise Schiff's base for ion recognition studies [20]. However, there is no report on anticancer studies by using these derivatives (**S1**-**S5**).

2. Experimental

2.1. General procedure for spectral measurement, binding studies (DNA, EtBr and BSA)

Both absorption and emission spectra were recorded on a UV–Vis spectrophotometer (JASCO V-730) and spectrofluorometer (FP-8200) using a 1 cm quartz cell. The DNA binding study was carried out by using ligands (**S1**-**S5**) in 5 mM Tris-HCl-NaCl buffer at pH 7.4 in phosphate buffer [21,22]. The intrinsic constant (K_b) was calculated using the equation (i).

$$\frac{DNA}{(\varepsilon_a - \varepsilon_f)} = \frac{DNA}{(\varepsilon_b - \varepsilon_f)} + \frac{1}{K_b(\varepsilon_a - \varepsilon_f)} \quad \text{(i)}$$

where ε_a, ε_f and ε_b are apparent extinction coefficient of ligand, extinction coefficient of the ligand in its free form and completely bound to DNA respectively.

The apparent association constant (K_{app}) of ligand to CT-DNA was established from the emission response using EtBr as a spectral probe 5 mM Tris-HCl-NaCl buffer at pH 7.4 [23]. The K_{app} was found by using the equation (ii)

$$K_{app} \times [Complex]_{50} = K_{EtBr} \times [EtBr] \quad \text{(ii)}$$

where $[\text{ligand}]_{50}$ represent the concentration of the complex at 50% quenching of DNA-bound EtBr emission intensity K_{EtBr} ($1.0 \times 10^7\ M^{-1}$) binding constant of EtBr, and concentration of EtBr was used 8 μM. The Stern-Volmer quenching constant (K_{SV}) was calculated from equation (iii) [24].

$$\frac{I_0}{I} = 1 + K_{SV}[Q] \quad \text{(iii)}$$

where I_0 and I are emission intensities of EtBr-DNA in the absence and in the presence of complex of concentration [Q].

The quantum yield (φ) was calculated according to comparative William's method in MTT condition [25]. The quantum yield was

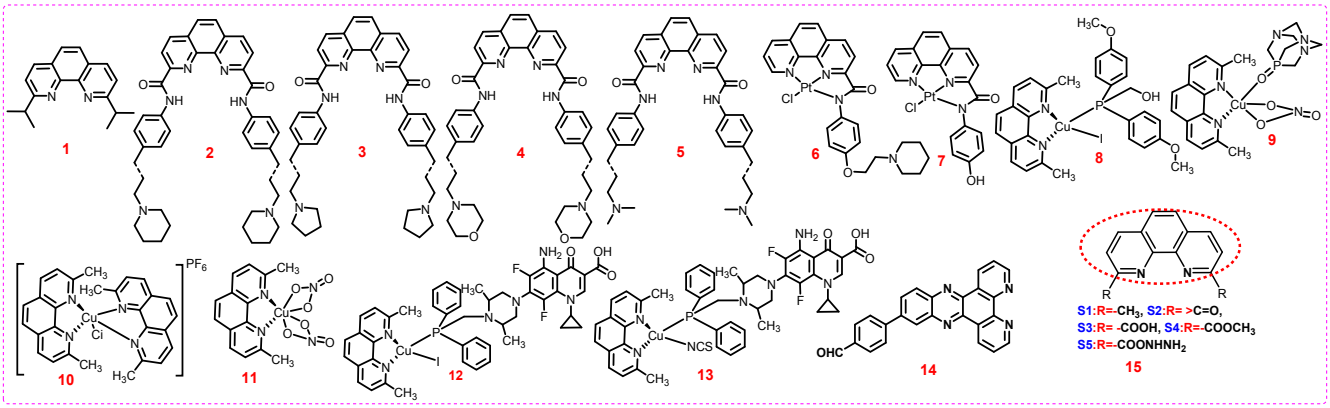

Fig. 1. . Molecular structure of phenanthroline derivatives previously reported in literature.

calculated according to the equation (iv)

$$\phi = \phi_R \times \frac{I_S}{I_R} \times \frac{OD_R}{OD_S} \times \frac{\eta_S}{\eta_R} \quad \text{(iv)}$$

where, φ, I, OD, and η represents quantum yield, peak area, absorbance recorded at $\lambda_{max,}$ and refractive index of solvent respectively.

The interaction of ligand with BSA has been calculated from tryptophan fluorescence quenching response [26]. Here, the ligand solution was incrementally added to BSA in Tris-HCl-NaCl buffer at pH 7.2. The SV quenching constant (K_{BSA}) of the fluorescence at 340 nm was calculated using equation (v and vi). Further, using Scatchard equation (vii), K and n values were calculated [27].

$$\frac{I_0}{I} = 1 + K_{BSA}[Q] = 1 + K_q \tau_0 [Q] \quad \text{(v)}$$

$$K_q = \frac{K_{BSA}}{\tau_0} \quad \text{(vi)}$$

$$\log \frac{I_0 - I}{I} = \log k + n \log[Q] \quad \text{(vii)}$$

where, I_0, I , k_q, τ_0, K and n represents emission intensities of BSA in the absence and in the presence of quencher of concentration [Q], quenching constant, average lifetime of tryptophan (1×10^{-8} s), binding constant and number of binding sites respectively [28].

2.2. Relative viscosity study

To find out the type of binding interaction of **S1-S5** with DNA was studied by viscosity measurements using Ostwald's viscometer. Each experiment was performed for three times and the average flow time was recorded. The data was plotted as $(\eta/\eta_0)^{1/3}$ vs. [ligand]/[DNA], where η and η_0 corresponds to viscosity of DNA in the presence of the ligand, and viscosity of DNA alone respectively. The viscosity of DNA was calculated using the formula $\eta_0 = (t\text{-}t_0)/t_0$ where t and t_0 represents the efflux time of DNA and PBS buffer solution respectively [29–31].

2.3. DNA degradation study

Initially, 0.15 g of plasmid DNA (~1 kb) was dissolved in 1 mL of Tris-HCl-NaCl buffer solution and further this solution was mixed with an equal volume of ligand (containing 1, 2 and 3 mg/ml). This solution mixture was incubated for 1 h at 37 °C and loaded on 1% agarose gel containing EtBr (1.0 mg/ml) and 2 mL buffer solution (containing 25% bromophenol blue, 30% glycerol and 0.25% xylene cyanol). Here, plasmid DNA was used as a positive control. The degradation experiment was carried out at 50 V for 60 min in buffer solution [32] and the gel plate was visualized using a gel documentation instrument.

2.4. In-vitro cytotoxic study

Each ligand was dissolved in 0.1% DMSO and then serial dilution with cell medium. Here, we have selected two different cancer cell lines such as HeLa, MDA-MB-231 and normal cell lines HEK-293 were used in this assay. The doxorubicin was used as a positive control with the same volume of medium. Hemocytometer was used for counting of cells. The amount of cell seeded was 1×10^4 cells per well in a 96 well plate. The entire cell lines was cultured in 100 μL of a growth medium in 96-well plates and incubated at 37 °C under 5% CO_2 overnight. After 24 h of incubation, the cultured cells were exposed to various concentrations of the ligands (**S1**-**S5**) (9–300 μM). After 24 h, the wells were treated with 10 μL MTT reagent (1 mg/ml) and incubated for 3 h at 37 °C. The suspension was retained on micro vibrator for 10 min and afterward the absorbance was calculated by the ELISA reader at λ_{max} (570 nm). The testing was executed in triplicate. The growth inhibition percentage was calculated according to the equation [33–35]: percentage growth inhibition = 100-[(AD × 100)/AB], where AD, measured absorbance in wells which contain samples and AB, measured absorbance for blank wells.

2.5. In-silico study and DFT theory

In order to know molecular interactions, each ligand was investigated for their binding affinities by molecular docking study using Autodock vina [36] along with the features of AutoDock Tools (ADT). In search of a smaller DNA section [d(CCGTCGACGG], an widely used oligodeoxynucleotide [37] (pdb entry: 423D) was fetched procured from Protein Data Bank (www.rcsb.org/pdb) [38]. 2D molecular skeleton of all five synthesized compounds (**S1**-**S5**) were developed using ACD ChemSketch Freeware. Further, 3D coordinates structures were built to make these fit to get into the subsequent stages of docking [39]. The binding site was mapped with a grid box with a spacing of 1 Å and 24 × 24 × 24 number of points was used in x y and z directions. Both the target and the compounds were tuned to introduce their pdbqt forms. The process yielded 9 poses for each ligand by considering the exhaustiveness of 8. Two aspects, *via* the scoring functions and close proximity between the conformer and active site residues were considered to assess the quality of all the bioactive conformers. Several orientations of each compound within the active site were observed using PyMOL (The PyMOL Molecular Graphics System, Version 1.3, Schrodinger, LLC) molecular graphics program. In an attempt to develop the virtual understanding of protein binding study and subsequently correlating it with the experimental study, molecular docking study was conducted with the 3D structure of BSA with PDB ID: 4F5S [40]. The protein structure was made free from water molecule so as to avoid the probability of undesired interaction. The other process was followed as similar as that of the earlier one. The grid box was placed considering the relative positions of two essential active site residues, *via*. Trp213 and Trp134 [41].

To calculate electronic properties of ligand, computational calculations was performed in the gas phase using density functional theory (DFT) by applying the Becke three-parameter Lee-Yang-Parr (B3LYP) exchange correlation functional. The basic set 6-311G(d,p) was used for all atoms. All the geometrical optimizations were done with zero negative vibrational frequency. The calculations were carried out using Gaussian 09 program [42].

3. Results and discussion

3.1. Synthesis and photo-physical studies of ligands

The synthesis of ligand **S5** follows four steps reaction *via* various intermediates such as 1,10-phenanthroline-2,9-dicarbaldehyde (**S2**), 1,10-phenanthroline-2,9-dicarboxylic acid (**S3**), 1,10-phenanthroline-

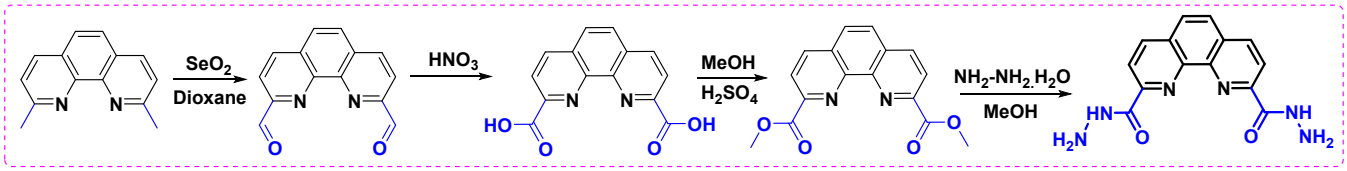

Scheme 1. Reagents and conditions to synthesize ligands **S2-S5.**

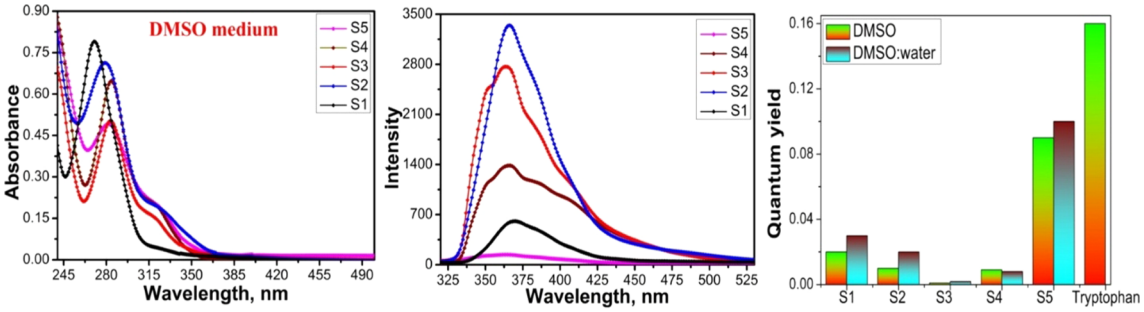

Fig. 2. . Absorption and emission spectral studies of **S1-S5** compounds (3×10^{-5} M*)* in DMSO medium.

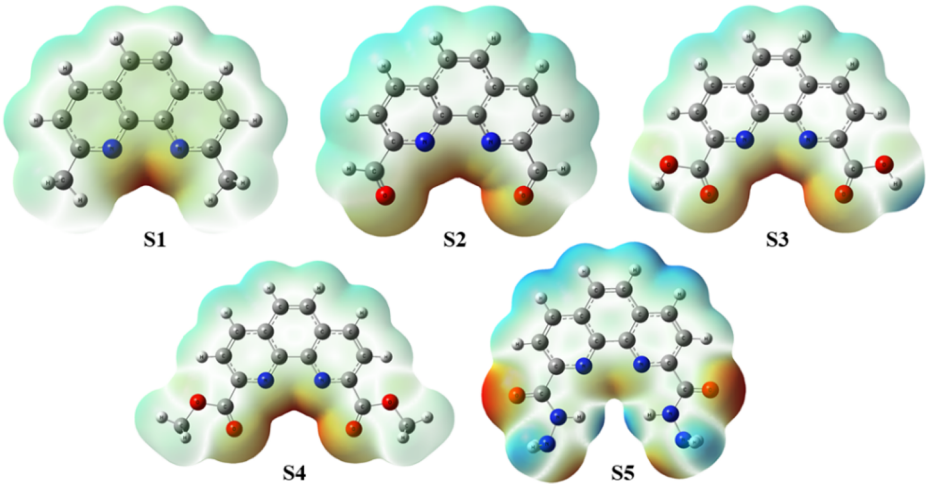

Fig. 3. . The ESP mapped on surface of ligands (**S1-S5**) by DFT-B3LYP method.

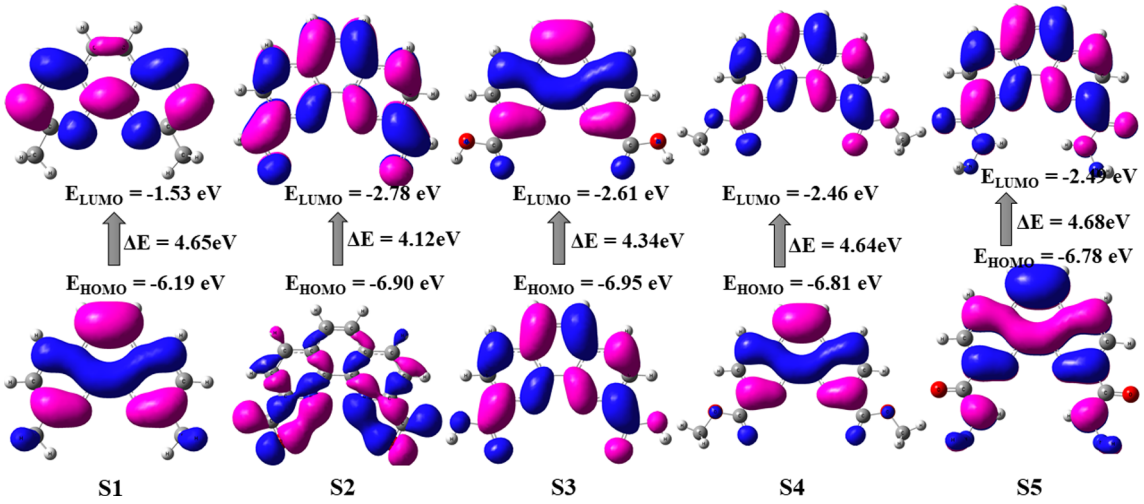

Fig. 4. . FMO's of ligands **(S1-S5)** by using DFT-B3LYP method.

Table 1
. Molecular electronic parameters of ligands (**S1-S5**) performed by DFT-B3LYP method.

Ligand	Energy (kJ/mol)	DM (Debay)	E_H (eV)	E_L (eV)	ΔE (eV)	χ (eV)	η (eV)	μ (eV)	ω (eV)	S (eV)
S1	−650	2.27	−6.19	−1.53	4.65	3.86	−2.33	−3.86	−3.20	−1.17
S2	−798	8.85	−6.90	−2.78	4.12	4.84	−2.06	−4.84	−5.69	−1.03
S3	−949	6.73	−6.95	−2.61	4.34	4.78	−2.17	−4.78	−5.26	−1.09
S4	−1028	6.02	−6.81	−2.46	4.36	4.64	−2.18	−4.64	−4.94	−1.09
S5	−1020	4.25	−6.87	−2.49	4.39	4.68	−2.19	−4.68	−5.00	−1.10

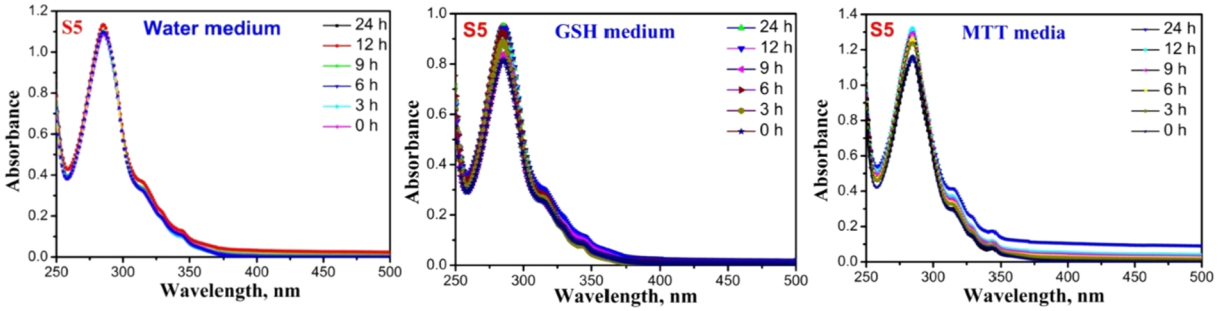

Fig. 5. . Stability studies of **S5** in natural physiological condition.

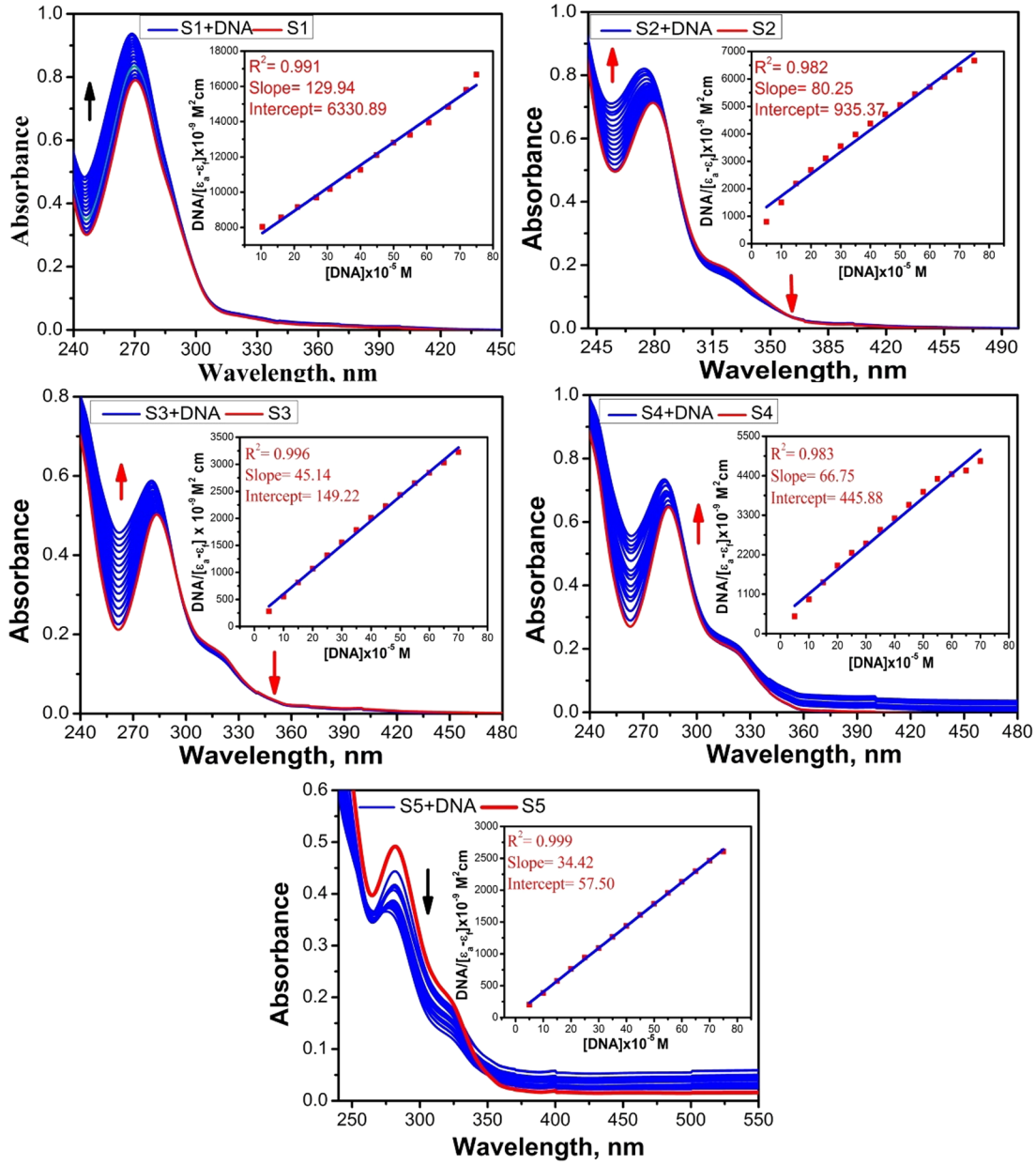

Fig. 6. . UV–visible spectral response of ligands (**S1-S5**) (3×10^{-5} M) in 5 mM tris-HCl-NaCl (pH, 7.2) with incremental addition of CT-DNA (3×10^{-5} M). Insert Fig. Linear plot used for calculating binding constant of ligand.

2,9-dicarboxylate (**S4**), and 1,10-phenanthroline-2,9-dicarbohydrazide (**S5**) were discussed in Scheme 1. Besides, **S3** and **S4** ligands are rich in oxygen atoms while **S5** rich in nitrogen atoms.

To work as a drug, given ligand has to acquire required lipophilicity. Therefore, the solubility of the ligand was performed in selected solvents from non-polar and polar solvents. The solubility reveals that all ligands were insoluble in chloroform and moderately soluble in water but good solubility was found in DMSO and DMF medium.

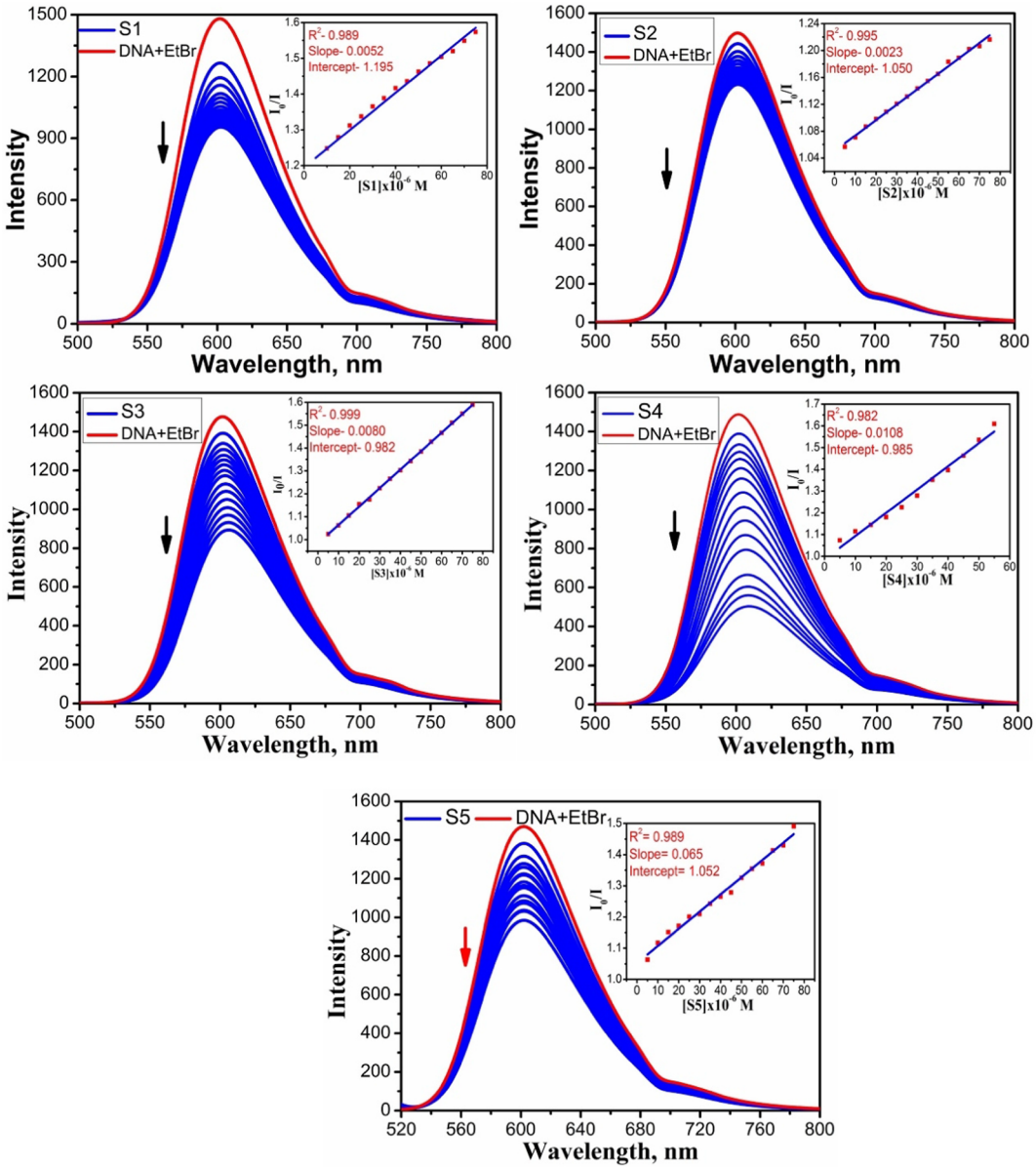

Fig. 7. . Fluorescence quenching curves of EtBr bound to DNA by (**S1-S5**) in Tris-HCl buffer solution (1×10^{-3} mol/L, pH = 7.2) at 298 K ([EtBr] = 8×10^{-6} mol/L; [DNA] = 1.2×10^{-4} mol/L; [**S1-S5**] = 3×10^{-5} mol/L; λ_{ex} = 485 and λ_{em} = 598 nm). Insert **Fig.** SV plot of each ligand.

The photo physical properties of ligand was performed by measuring absorbance and emission in DMSO and MTT environment. The spectral studies revealed that high energy band appeared in the region of 273–300 nm owing to ligand centered $\pi \rightarrow \pi^*$ transitions shown in Fig. 2. The emission ability of each ligand was studied at respective wavelength maximum as their excitation energy. The maximum emission was in the range of 330–510 nm. Further, the quantum yield of all ligands exhibit high in DMSO medium and the order of yield was found to be **S5** > **S1** > **S2** > **S3** > **S4**.

In order to support experimental results, theoretical studies were performed using DFT, various quantum-chemical parameters were calculated by applying B3LYP/6-311G** such as molecular energy, electrostatic potential charges, and energy of HOMO/LUMO to calculate energy gap [43]. The electrostatic potential mapped onto the constant electron density surface. The 3D plot of molecular electrostatic potential of **S1**-**S5** were shown in Fig. 3. The maximum negative region (red colour) and positive region (blue colour) are preferred sites for electrophilic and nucleophilic attack respectively. In **S1**-**S4**, the negative ESP is more on the phenanthroline semi cavity whereas in ligand **S5,** it is more at outside the semi cavity. The energies of the FMOs describe the molecule's ability to donate and accept an electron (ΔE) shown in Fig. 4, electronegativity (χ), chemical potential (μ), global hardness (η), global softness (S) and global electrophilicity index (ω) were listed in Table 1 [44–46]. The significant of these parameters is to measure the molecular stability and reactivity of the ligands. The molecular electronic properties of ligands (**S1**-**S5**) reveals that these ligands acquired these properties which make suitable for nucleic acid interactions [47]. However, the electrophilicity quantifies the biological activity of ligand.

For unique therapeutics initiative, ligand has to be stable inside the cells in internal physiological condition. Hence, in order to know the stability in such environment, ligand **S5** has selected for stability test and it was performed in pure water, 0.1 mM GSH and MTT environment by using UV–Vis spectrophotometer for about 24 h (Fig. 5). It reveals that in all three medium, ligand **S5** remain same in terms of absorbance and wavelength maximum even after 24 h contact which establishes it's utility in biological system.

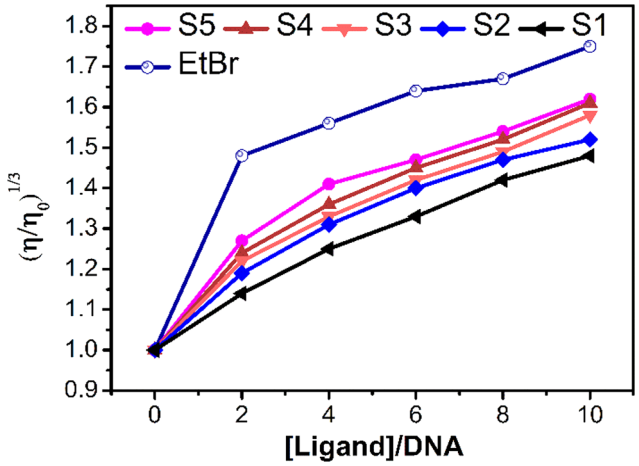

Fig. 8. Effect of increasing amounts of ligands (**S1-S5**) on the viscosity of CT-DNA at 298 K ([EtBr] = 1 × 10^{-6} mol/L; [DNA] = 1 × 10^{-6} mol/L; [Ligand] = 1 × 10^{-3} mol/L).

3.2. DNA binding study

The ligand-DNA interaction can be observed by change in absorbance maxima owing to strong π-π stacking between DNA base pairs and phenanthroline core. The absorption spectra of all ligands were observed at 268 nm while neat CT-DNA seems a broad band (230–296 nm) with a wavelength maximum at 258 nm. DNA base pairs (adenine, guanine, cytosine and thymine) are mainly accountable for this electronic transition. In ligands **S1-S4**, on increasing the CT-DNA, hyperchromism effect was observed due to DNA duplex has denatured, and ligand well intact with DNA which facilitates more light to be absorbed by the ligand. In case of **S5**, it exhibits hypochromic effect due to intercalation in DNA helix and hence the amount of light absorbed by ligand will be less. The intrinsic DNA binding constant (K_b) of each ligand was calculated from the plot [DNA]/(ε_a-ε_f) vs. [DNA]. Accordingly, the K_b value of **S1-S5** were found to be 2.1 × 10^4 M^{-1}, 8.6 × 10^4 M^{-1}, 3.1 × 10^5 M^{-1}, 3.5 × 10^5 M^{-1}, 5.9 × 10^5 M^{-1} respectively (Fig. 6). The obtained K_b value revealed that ligand **S5** showed higher binding affinity towards DNA in comparison with rest of the ligands.

3.3. EtBr displacement study

Competitive binding studies of **S1-S5** with CT-DNA was calculated by using spectrofluorimetric in the presence of EtBr. It is a highly sensitive emissive sensor which interrelates with DNA *via* π-π* intercalation. The introduction of new ligand in the EtBr-DNA molecular assembly results in decrease of emission intensity due to displacement of EtBr from the DNA double helix. The ability of fluorescence quenching of EtBr pre-treated DNA might be used to determine the apparent binding constant (K_{app}) of the ligand with CT-DNA by using excitation energy 485 nm fluorescence emission was recorded at 598 nm (Fig. 7). The 50% quenching of DNA-EtBr occurred at concentration of 30–37.5 μM. The SV quenching constant of **S1-S5** was found to be 5.2 × 10^3 M^{-1}, 2.3 × 10^3 M^{-1}, 8.0 × 10^3 M^{-1}, 1.1 × 10^4 M^{-1}, 6.5 × 10^4 M^{-1} respectively which is low as compared to the known intercalators. Among five ligands studied, **S4** and **S5** have showed high order intercalation tendency compare to other ligands (**S1-S3**) owing to more electrostatic and groove binding with DNA.

3.4. Viscosity study

To identify mode of interaction of **S1-S5** with DNA, viscosity responses were carried out with CT-DNA by different concentration of **S1** to **S5** ligands. The ligands have to quandary with the DNA double helix and separate the adjacent base pairs *via* intercalation mode thereby consecutively an increase in the length and viscosity of DNA. As seen from Fig. 8, there is an increase in relative viscosity with increasing in concentration of ligand. The order of increasing in viscosity follows: **S5** > **S4** > **S3** > **S2** > **S1** this might be due to intercalation of the ligand.

3.5. DNA degradation study

The DNA degradation experiment of the ligands (**S1-S5**) was studied by using agarose gel electrophoresis (Fig. 9). The cleavage studied was done using three different concentration (containing 1, 2 and 3 mg/ml). The control plasmid DNA was arranged in two conformations where the upper and lower bands match to the nicked and supercoiled forms. The study reveals that the plasmid DNA (≈1 kb) was degraded within 1.5 h by all ligands at 3 mg/ml while ligands **S4** and **S5** were also found degrade even at 2 and 1 mg/ml and even in 1 mg/ml. This degrading efficiency of ligands (**S4** and **S5**) may be due to disrupt the double and triple hydrogen bonds formed between the nucleotide bases.

3.6. Protein binding study

The binding interaction of ligand**s (S1-S5)** with BSA was studied by using intrinsic tryptophan emission quenching of BSA. Upon increase in concentration of ligand, the quenching of BSA was decreased gradually (Fig. 10). This may be due to several molecular interactions and perturbation in the secondary structure of the protein upon interaction with ligand. In case of ligands (**S1-S4**), a minor red shift of 10–50 nm of emission maximum was observed. This could be due to an increase in hydrophobicity of the microenvironment around the tryptophan residues leads [48]. These variations happened owing to ligand-protein interaction leads to disruption of protein tertiary structure and hence losses its activity [49,50]. Therefore, ligands (**S1-S4**) showing destruction of tertiary structure of protein due to damage of charged amino acid side chain interaction while **S5** ligand exhibits secondary structure damage due to destruction of hydrogen bonding (carbonyl oxygen of amino acid and the amino hydrogen of ligand **S5**) which is an important factor. In order to quantify these interactions, the SV quenching constant (K_{BSA}), quenching rate constant (K_q) were calculated from slope of

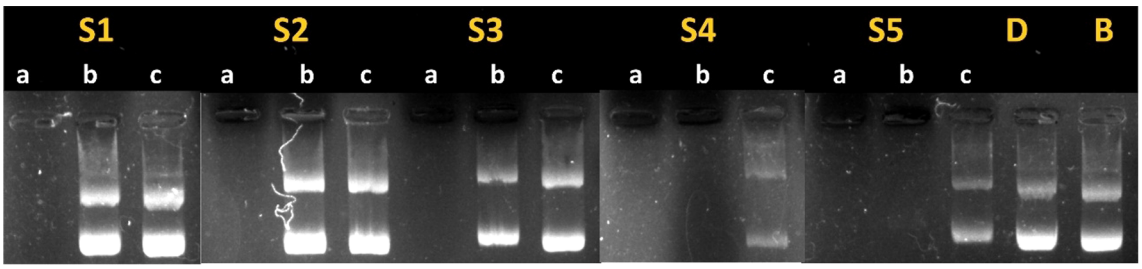

Fig. 9. . Gel electrophoresis diagram showing chemical nuclease activity of **S1** to **S5:** Lane B: PBS Buffer solution; Lane D: pure DMSO; Lane **S1-S5**: containing (a) 3 mg/ml (b) 2 mg/ml and (c) 1 mg/ml.

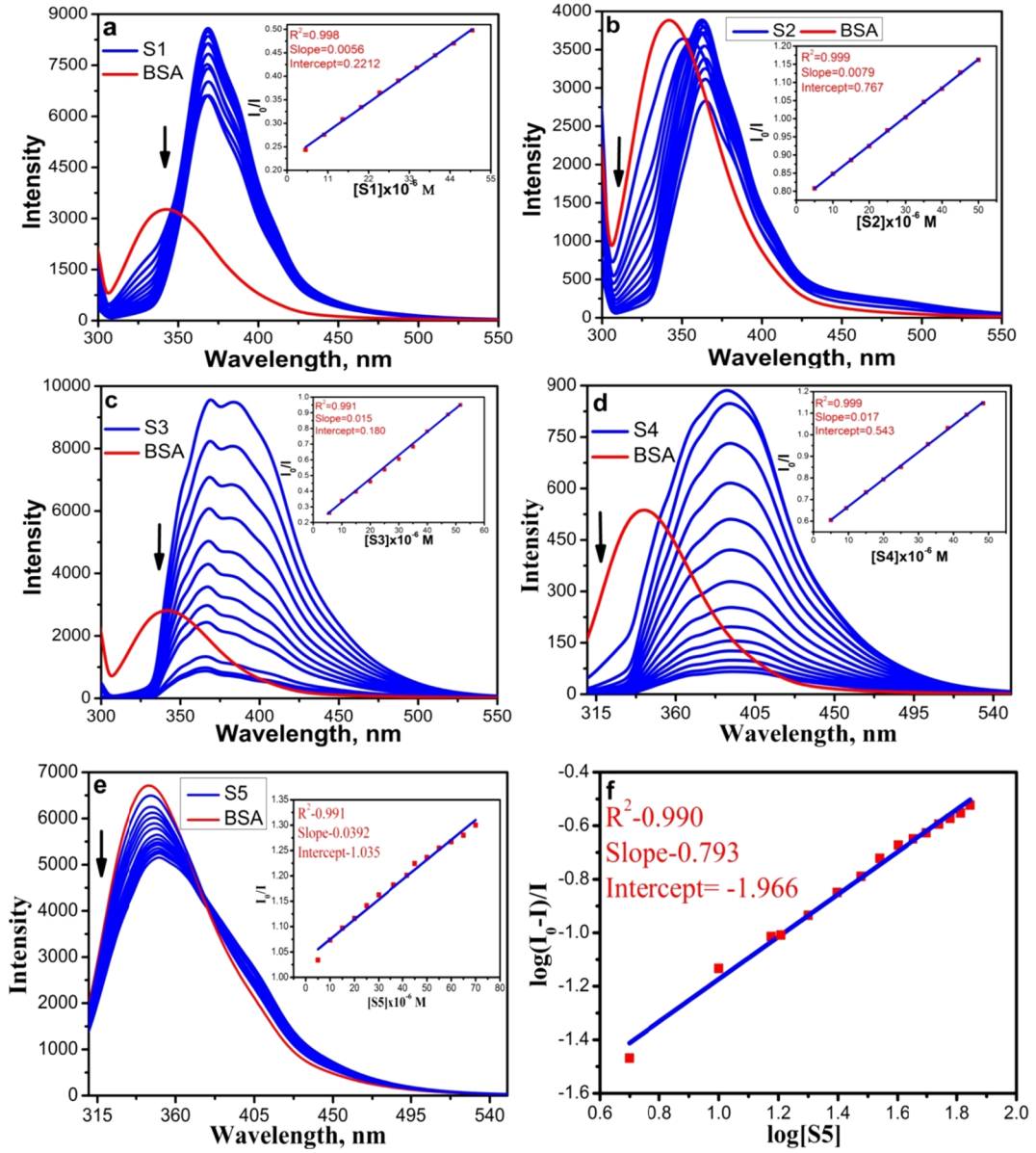

Fig. 10. . Fluorescence quenching of BSA on addition of ligands (a-e, **S1-S5**) in 5 mM Tris HCl/NaCl buffer at pH 7.2 (λ_{ex} = 295 nm; λ_{em} = 350 nm). (e) Inserted figure, SV plot of I_0/I vs. [**S5**] (f) Scatchard plot of log ($[I_0\text{-}I]/I$) vs. log [**S5**].

Table 2
. Docking studies of ligands (**S1**-**S5**) with DNA and BSA.

Ligand	Binding free energy ($\Delta G_{binding}$)[α]	Vdw_hb_desolv energy ($\Delta G_{vdW+hb+desolv}$)	Electrostatic energy (ΔG_{elec})	Total internal energy (ΔG_{total})	Torsional free energy (ΔG_{tor})	Unbound system's energy (ΔG_{unb})
(a) DNA						
S1	−7.2	−6.7	−0.83	0.73	0.33	−0.73
S2	−6.9	−6.4	−0.62	−0.94	0.12	−0.94
S3	−7.3	−6.9	−0.57	−1.12	0.17	−1.12
S4	−7.5	−6.9	−0.88	−1.01	0.28	−1.01
S5	−7.9	−7.4	−0.71	−1.03	−0.21	−1.03
(b) BSA						
S1	−7.1	−6.7	−0.58	−0.89	0.28	−0.89
S2	−7.5	−6.9	−0.67	−1.09	0.07	−1.09
S3	−7.7	−7.2	−0.72	−0.99	0.22	−0.99
S4	−8.4	−7.9	−0.75	−1.12	0.25	−1.12
S5	−8.6	−8.1	−0.69	−1.04	0.19	−1.04

[α] $\Delta G_{binding} = \Delta G_{vdW+hb+desolv} + \Delta G_{elec} + \Delta G_{total} + \Delta G_{tor} - \Delta G_{unb}$ (expressed in terms of Kcal/mol).

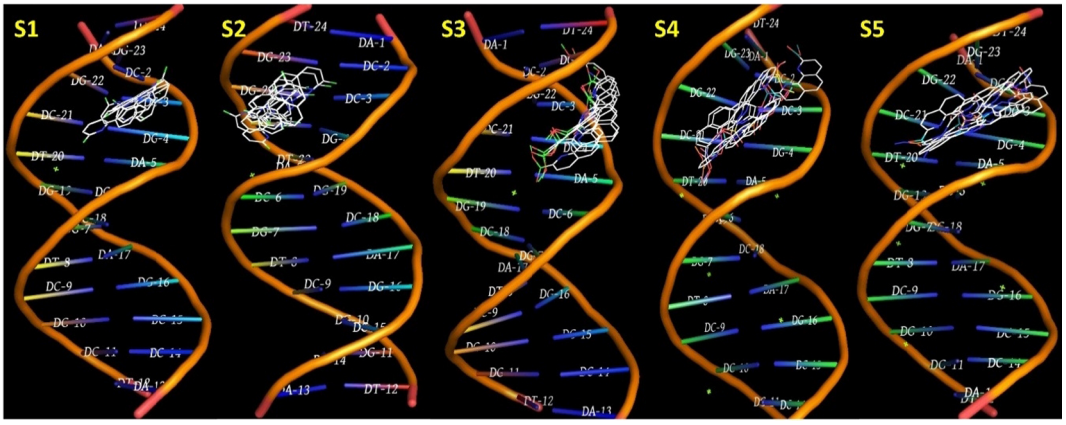

Fig. 11. . Docking pose of **S1** to **S5** within the minor groove of DNA.

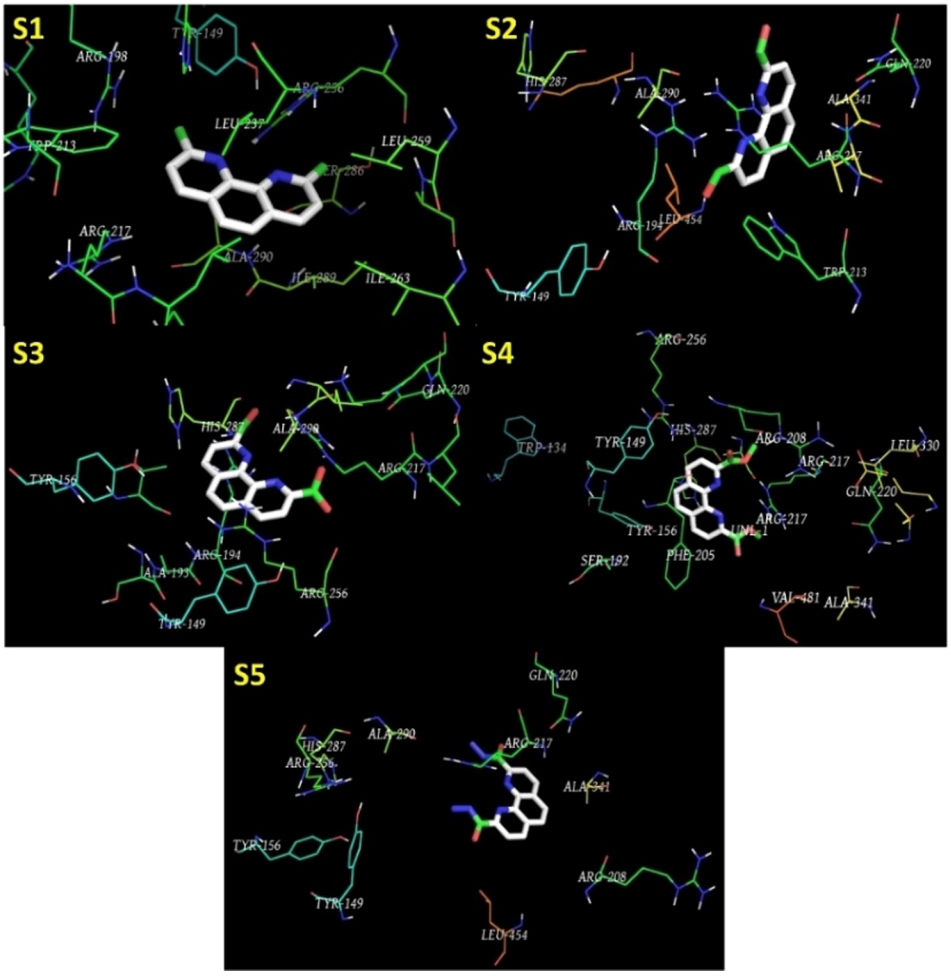

Fig. 12. . Docking pose of **S1**-**S5** within the active site of BSA protein.

the linear plot of I_0/I vs. [ligand]. The order of increasing in K_{BSA} follows: **S5** > **S4** > **S3** > **S2** > **S1** this might be due to intercalation of the ligand. This may be due to more electrostatic interaction is expected in **S5** ($3.9 \times 10^4\ M^{-1}$), **S4** ($1.7 \times 10^4\ M^{-1}$) and **S3** ($1.5 \times 10^4\ M^{-1}$) compare to corresponding **S2** ($7.9 \times 10^3\ M^{-1}$) and **S1** ($5.6 \times 10^3\ M^{-1}$). The binding affinity (K) and number of binding sites (n) of ligand **S5** was found to be $1.4 \times 10^5\ M^{-1}$ and 0.79 respectively. The obtained K_{BSA} value revealed that ligand **S5** showed higher binding affinity towards BSA in comparison with rest of the ligands. These binding characteristics showing a binding tendency with BSA which is a crucial for transportation of protein-bound complexes in biological systems.

3.7. In-silico study

Molecular docking studies of synthesized ligands (**S1**-**S5**) were carried out with the DNA duplex consisting of d(CGCGAATTCGCG) dodecamer sequence. Scoring functions/binding energy, one of the important parameter for prioritizing the efficiency of all the docked compounds was given in Table 2(a). DNA binding study reveals that ligand **S5** ranked to be the 1st owing to its highest binding energy

Table 3
. MTT cytotoxicity screening of ligands (**S1-S5**) at 24 h of exposure.

Ligand	Cell Line (*IC_{50} μM)			Selectivity factor**	
	HeLa	MDA-MB-231	HEK-293	HeLa	MDA-MB-231
S1	37.47 ± 1.2	57.03 ± 1.3	97.12 ± 1.6	2.59	1.70
S2	31.69 ± 1.8	66.12 ± 1.9	121.38 ± 2.1	3.83	1.83
S3	35.87 ± 1.3	68.75 ± 1.6	94.62 ± 1.5	2.63	1.37
S4	64.66 ± 2.2	13.35 ± 1.1	82.75 ± 1.9	1.27	6.19
S5	7.66 ± 1.1	19.23 ± 1.4	99.42 ± 1.4	12.97	5.17
Doxorubicin	19.71 ± 1.2	20.22 ± 1.6	74.21 ± 1.1	3.76	3.67

* IC_{50} is the concentration at which 50% of cells undergoes cytotoxic cell death under treatment.

** Selectivity factor: ratio of IC_{50} for HEK-293 and IC_{50} for all the cancer cell lines. HEK-293 fibroblasts are generally selected as the model for healthy cells in the evaluation of chemotherapeutic drug selectivity.

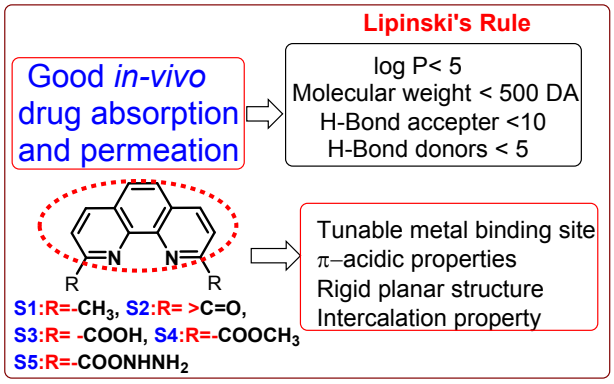

Fig. 13. . SAR of phenanthroline derivatives (**S1-S5**).

(−8.6 kcal/mol). The binding energy can be well correlated with the docking pose obtained for the same ligand as shown in Fig. 11. The cluster of conformers are lying well within the base pairs, thus could be a better candidate as DNA intercalator. The other ligands in the same series also possess near equal poses with the target DNA. On the other hand, Table 2(b) consists of the binding energy of the same series of ligands employed for the BSA binding study. From an overall perusal of literature, it is observed that the important amino acids constitute active site of bovine serum albumin are Tyr137, Tyr149, Tyr156, Phe205, Arg208, Arg217, Ala290, Ala341 etc. Ligand **S5** being the highly active one as DNA intercalator, scores highest (binding energy: −7.9 kcal/mol) against the protein as well. The docking poses as shown in Fig. 12 implied that respective conformer of each compound are held strongly by the active site residues. Thus, it is inferred that docking study serves as an important linker between ideation of the proposal and execution of the work.

3.8. MTT cytotoxicity test

In this assay, living cells reduce the yellow MTT to insoluble purple formazan crystals. All ligands were dissolved in DMSO. The cytotoxicity studies of ligands **S1-S5** were examined by using MTT method using cell lines such as MDA-MB-231, HeLa and HEK-293. Cells were well-maintained with ligands along with doxorubicin as a standard positive control with various concentrations from 9 μM −300 μM for 24 h. DMSO was used as a control and it didn't disturb any inhibition of cancer cell growth. The anti-proliferative activity of the ligands based on the half maximal inhibitory concentrations (IC_{50} values) is shown in Table 3. The IC_{50} values of ligands with HeLa and MDA-MB-231 cells follows an order: **S5** < **doxorubicin** < **S4** < **S3** < **S2** < **S1** and **S4** < **S5** < **doxorubicin** < **S3** < **S2** < **S1** were observed respectively. This high potency of **S4** and **S5** were caused by more rapid diffusion into cell as a result there is enhanced intracellular ligand concentration, which eventually led to the stronger cytotoxicity. Besides, all these ligands exhibits least effect to normal cells compare to standard drug used in this study. The cytotoxicity performance of organometallic complex based on 2,9 substituted phenanthroline (16–18) have shown high anticancer agent properties compare to 2,9 substituted phenanthroline ligands (13,14). However, the selectivity factor of ligands **S4** and **S5** are found to be high compare to reported work.

3.9. Structure activity relationship

SAR was performed according to the results of cytotoxicity of the evaluated compounds. Among five compounds **S5** and **S4** were exhibits an excellent IC_{50} values in the studied ligands including standard drug doxorubicin. Further, on comparing selectivity factor, ligand **S5** and **S4** exhibits highest selectivity while remaining three ligands (**S1-S3**) and standard drug shows almost same factor. One of the key future of ligands (**S1-S5**) is that phenanthroline core will provide rigidity, planarity, aromaticity, basicity, rotatable bonds, low molecular weight and hydrophobic nature enrich the cellular accumulation. Hence, these ligands are reasonably a worthy to use as cytotoxic agents (Fig. 13).

4. Conclusion

In summary, we have designed and synthesized four 2,9 substituted 1,10 phenanthroline as rigid derivatives and to evaluated as cytotoxicity against two cancer cell lines. The stability test revealed that ligand is stable in all three (water, GSH and MTT) selected media. Both experimental and computation studies shows that all ligands have good binding affinity with nucleic acids. The gel electrophoresis studies exhibited that **S4** and **S5** have cleaved plasmid DNA completely within 60 min. Ligands **S5** and **S4** showed least IC_{50} values and high selectivity factor with selected HeLa and MDA-MB-231 cell lines respectively. Therefore, in conclusion, we believe that ligands **S5** and **S4** have an important role for displaying the cytotoxic effects.

CRediT authorship contribution statement

Sourav De: Conceptualization, Methodology. **S.K. Ashok Kumar:** Investigation, Writing - original draft.

Declaration of Competing Interest

The authors declare that they have no known competing financial interests or personal relationships that could have appeared to influence the work reported in this paper.

Acknowledgements

Authors are grateful to Department of Science and Technology, Government of India for supporting the work through the project grant (EMR/2017/000816). Authors are also thankful to DST-VIT-FIST for NMR and GC-MS for research facilities. The authors are grateful to VIT for providing VIT SEED funding.

References

[1] D. Richards, A. Rodger, Synthetic metallomolecules as agents for the control of DNA structure, Chem. Soc. Rev. 36 (2007) 471–483.
[2] A. Bencini, V. Lippolis, 1, 10-Phenanthroline: a versatile building block for the construction of ligands for various purposes, Coord. Chem. Rev. 254 (2010) 2096–2180.
[3] G. Accorsi, A. Listorti, K. Yoosaf, N. Armaroli, 1, 10-Phenanthrolines: versatile building blocks for luminescent molecules, materials and metal complexes, Chem. Soc. Rev. 38 (2009) 1690–1700.
[4] L. Viganor, O. Howe, P. McCarron, M. McCann, M. Devereux, The antibacterial

activity of metal complexes containing 1, 10-phenanthroline: potential as alternative therapeutics in the era of antibiotic resistance, Curr. Top. Med. Chem. 17 (2017) 1280–1302.
[5] A. Airinei, R. Tigoianu, R. Danac, C.M. Al Matarneh, D.L. Isac, Steady state and time resolved fluorescence studies of new indolizine derivatives with phenanthroline skeleton, J. Lumin. 199 (2018) 6–12.
[6] C. Sall, A.D. Yapi, N. Desbois, S. Chevalley, J.M. Chezal, K. Tan, J.C. Teulade, A. Valentin, Y. Blache, Design, synthesis, and biological activities of conformationally restricted analogs of primaquine with a 1, 10-phenanthroline framework, Bioorg. Med. Chem. Lett. 18 (2008) 4666–4669.
[7] A. Rezvani, H.S. Bazzi, B. Chen, F. Rakotondradany, H.F. Sleiman, Ruthenium (II) dipyridoquinoxaline-norbornene: synthesis, properties, crystal structure, and use as a ROMP monomer, Inorg. Chem. 43 (2004) 5112–5119.
[8] K. Binnemans, P. Lenaerts, K. Driesen, C. Gorller-Walrand, A luminescent tris (2-thenoyltrifluoroacetonato) europium (III) complex covalently linked to a 1, 10-phenanthroline-functionalised sol–gel glass, J. Mater. Chem. 14 (2004) 191–195.
[9] P. Lenaerts, A. Storms, J. Mullens, J. D'Haen, C. Gorller-Walrand, K. Binnemans, K. Driesen, Thin films of highly luminescent lanthanide cosmplexes covalently linked to an organic-inorganic hybrid material via 2-substituted imidazo [4, 5-f]-1, 10-phenanthroline groups, Chem. Mater. 17 (2005) 5194–5201.
[10] A.M. Thomas, A.D. Naik, M. Nethaji, A.R. Chakravarty, Synthesis, crystal structure and photo-induced DNA cleavage activity of ternary copper (II)-thiosemicarbazone complexes having heterocyclic bases, Inorg. Chim. Acta. 357 (2004) 2315–2323.
[11] P. Hazarika, B. Bezbaruah, P. Das, O.K. Medhi, C. Medhi, A model study on the stacking interaction of phenanthroline ligand with nucleic acid base pairs: an ab initio, MP2 and DFT studies, J. Biophys. Chem. 2 (2011) 152–157.
[12] S.V. Kumar, T.D. Sakore, H.M. Sobell, Structure of a novel drug-nucleic acid crystalline complex: 1,10-phenanthroline-platinum(II) ethylenediamine-5′-phosphorylthymidylyl (3′-5′) deoxyadenosine, J. Biomol. Struct. Dyn. 2 (1984) 333–344.
[13] D. Wang, S. Peng, A.R.M.R. Amin, M.A. Rahman, S. Nannapaneni, Y. Liu, D.M. Shin, N.F. Saba, J.F. Eichler, Z.G. Chen, Antitumor activity of 2, 9-Di-Sec-Butyl-1, 10-Phenanthroline, PLoS ONE 11 (2016) e0168450.
[14] L. Wang, Y. Wen, J. Liu, J. Zhou, C. Li, C. Wei, Promoting the formation and stabilization of human telomeric G-quadruplex DNA, inhibition of telomerase and cytotoxicity by phenanthroline derivatives, Org. Biomol. Chem. 9 (2011) 2648–2653.
[15] J.E. Reed, S. Neidle, R. Vilar, Stabilisation of human telomeric quadruplex DNA and inhibition of telomerase by a platinum–phenanthroline complex, Chem. Commun. 4366–4368 (2007).
[16] U.K. Komarnicka, S. Kozieł, P. Zabierowski, R. Kruszyński, M.K. Lesiów, F. Tisato, M. Porchia, A. Kyzioł, Copper (I) complexes with phosphines P (p-OCH3-Ph) 2CH2OH and P (p-OCH3-Ph) 2CH2SarGly. synthesis, multimodal DNA interactions, and prooxidative and in vitro antiproliferative activity, J. Inorg. Biochem. 203 (2020) 110926.
[17] E.I. Sliwa, U. Sliwinska-Hill, B. Bazanow, M. Siczek, J. Klak, P. Smolenski, Synthesis, structural, and cytotoxic properties of new water-soluble copper (II) complexes based on 2, 9-dimethyl-1, 10-phenanthroline and their one derivative containing 1, 3, 5-Triaza-7-Phosphaadamantane-7-Oxide, Molecules 25 (2020) 741.
[18] A. Kyziol, A. Cierniak, J. Gubernator, A. Markowski, M. Jezowska-Bojczuk, U.K. Komarnicka, Copper (I) complexes with phosphine derived from sparfloxacin. Part III: multifaceted cell death and preliminary study of liposomal formulation of selected copper (I) complexes, Dalton Trans. 47 (2018) 1981–1992.
[19] S. De, B. Sarkar, G.R. Jadhav, S.K. Ramasamy, S. Banerjee, A. Moorthy, P. Paira, S.K. Ashok Kumar, Experimental and Theoretical Study on the Biomolecular Interaction of Novel Acenaphtho Quinoxaline and Dipyridophenazine Analogues, ChemistrySelect 3 (2018) 10593–10602.
[20] R. Selva Kumar, S.K. Ashok Kumar, K. Vijayakrishna, A. Sivaramakrishna, C.V.S.R. Brahmmananda, N. Sivaraman, S.K. Sahoo, Development of the smartphone-assisted colorimetric detection of thorium by using New Schiff's base and its applications to real time samples, Inorg. Chem. 57 (2018) 15270–15279.
[21] S. De, S. R. Chaudhuri, A. Panda, G. R. Jadhav, R. S. Kumar, P. Manohar, N. Ramesh, A. Mondal, A. Moorthy, S. Banerjee, S. K. Ashok Kumar, P. Paira, Synthesis, characterisation, molecular docking, biomolecular interaction and cytotoxicity studies of novel ruthenium (II)–arene-2-heteroarylbenzoxazole complexes, New J. Chem., 43 (2019) 3291-3302.
[22] K. Singh, S. Banerjee, A.K. Patra, Photocytotoxic luminescent lanthanide complexes of DTPA–bisamide using quinoline as photosensitizer, RSC Adv. 5 (2015) 107503–107513.
[23] S. Dasari, A.K. Patra, Luminescent europium and terbium complexes of dipyridoquinoxaline and dipyridophenazine ligands as photosensitizing antennae: structures and biological perspectives, Dalton Trans. 44 (2015) 19844–19855.
[24] J. Keizer, Nonlinear fluorescence quenching and the origin of positive curvature in Stern-Volmer plots, JACS 105 (1983) 1494–1498.
[25] M. Shamsi-Sani, F. Shirini, M. Abedini, M. Seddighi, Synthesis of benzimidazole and quinoxaline derivatives using reusable sulfonated rice husk ash (RHA-SO 3 H) as a green and efficient solid acid catalyst, Res. Chem. Intermed. 42 (2016) 1091–1099.
[26] V.D. Suryawanshi, L.S. Walekar, A.H. Gore, P.V. Anbhule, G.B. Kolekar, Spectroscopic analysis on the binding interaction of biologically active pyrimidine derivative with bovine serum albumin, J. Pharm. Anal. 6 (2016) 56–63.
[27] J. Liu, J. Tian, W. He, J. Xie, Z. Hu, X. Chen, Spectrofluorimetric study of the binding of daphnetin to bovine serum albumin, J. Pharm. Biomed. Anal. 35 (2004) 671–677.
[28] S. De, S.K. Subran, S.K. Ramasamy, S. Banerjee, P. Paira, S.K. Ashok Kumar, Luminescent anticancer acenaphtho[1, 2-b]quinoxaline: green synthesis, DFT and molecular docking studies, live-cell imaging and reactivity towards nucleic acid and protein BSA, ChemistrySelect. 3 (2018) 5421–5430.
[29] S. Banerjee, I. Pant, I. Khan, P. Prasad, A. Hussain, P. Kondaiah, A.R. Chakravarty, Remarkable enhancement in photocytotoxicity and hydrolytic stability of curcumin on binding to an oxovanadium (IV) moiety, Dalton Trans. 44 (2015) 4108–4122.
[30] S. Satyanarayana, J.C. Dabrowiak, J.B. Chaires, Neither. DELTA.-nor. LAMBDA.-tris (phenanthroline) ruthenium (II) binds to DNA by classical intercalation, Biochemistry 31 (1992) 9319–9324.
[31] R.K. Vuradi, K. Dandu, P.K. Yata, R.R. Mallepally, N. Chintakuntla, R. Ch, S.S. Thakur, C.M. Rao, S. Satyanarayana, Studies on the DNA binding and anticancer activity of Ru (ii) polypyridyl complexes by using a (2-(4-(diethoxymethyl)-1 H-imidazo [4, 5-f][1, 10] phenanthroline)) intercalative ligand, New J. Chem. 42 (2018) 846–859.
[32] A. Chandra, K. Singh, S. Singh, S. Sivakumar, A.K. Patra, A luminescent europium (III)–platinum (II) heterometallic complex as a theranostic agent: a proof-of-concept study, Dalton Trans. 45 (2016) 494–497.
[33] B.A. Lakshmi, J.Y. Bae, J.H. An, S. Kim, Facile design and spectroscopic characterization of novel bio-inspired Quercetin-conjugated tetrakis (dimethylsulfoxide) dichlororuthenium (II) complex for enhanced anticancer properties, Inorg. Chim. Acta 495 (2019) 118989.
[34] A. Mondal, S. De, S. Maiti, B. Sarkar, S.K. Ashok Kumar, R. Jacob, A. Moorthy, P. Paira, Amberlite IR-120 (H) mediated "on water" synthesis of fluorescent Ruthenium(II)-arene 8-hydroxyquinoline complexes for cancer therapy and live cell imaging, J Photochem. Photobiol. 178 (2018) 380–394.
[35] D. Smilowicz, N. Metzler-Nolte, Bioconjugates of Co(III) complexes with Schiff base ligands and cell penetrating peptides: Solid phase synthesis, characterization and antiproliferative activity, J. Inorg. Biochem. 206 (2020) 111041.
[36] O. Trott, A.J. Olson, AutoDock Vina: improving the speed and accuracy of docking with a new scoring function, efficient optimization, and multithreading, J. Comput. Chem. 31 (2010) 455–461.
[37] H. Rozenberg, D. Rabinovich, F. Frolow, R.S. Hegde, Z. Shakked, Structural code for DNA recognition revealed in crystal structures of papillomavirus E2-DNA targets, Proc. Natl. Acad. Sci. U.S.A. 95 (1998) 15194–15199.
[38] P.W. Rose, A. Prlic, C. Bi, W.F. Bluhm, C.H. Christie, S. Dutta, R.K. Green, D.S. Goodsell, J.D. Westbrook, J. Woo, The RCSB Protein Data Bank: views of structural biology for basic and applied research and education, Nucleic Acids Res. 43 (2015) D345–D356.
[39] N.M. O'Boyle, M. Banck, C.A. James, C. Morley, T. Vandermeersch, G.R. Hutchison, Open Babel: An open chemical toolbox, J. Cheminf. 3 (2011) 33.
[40] A. Bujacz, Structures of bovine, equine and leporine serum albumin, Acta Crystallogr, Sect. D: Biol. Crystallogr. 68 (2012) 1278–1289.
[41] G. Sudlow, D.J. Birkett, D.N. Wade, The characterization of two specific drug binding sites on human serum albumin, Mol. Pharmacol. 11 (1975) 824–832.
[42] M.J. Frisch, G.W. Trucks, H.B. Schlegel, Gaussian, Inc, Wallingford CT, 2009.
[43] E. Scrocco, J. Tomasi, Electrostatic molecular potential analysis of electron density distribution in (ClAlMe2) 2 and (AlCl3) 2, Adv Quantum Chem. 11 (1978) 115–121.
[44] M. Govindarajan, S. Periandy, K. Carthigayen, FT-IR and FT-Raman spectra, thermo dynamical behavior, HOMO and LUMO, UV, NLO properties, computed frequency estimation analysis and electronic structure calculations on α-bromotoluene, Spectrochim Acta, Part A 97 (2012) 411–422.
[45] R.G. Pearson, Absolute electronegativity and hardness: applications to organic chemistry, J. Org. Chem. 54 (1989) 1423–1430.
[46] J. Padmanabhan, R. Parthasarathi, V. Subramanian, P.K. Chattaraj, Electrophilicity-based charge transfer descriptor, J. Phys. Chem. A 111 (2007) 1358–1361.
[47] R. Parthasarathi, J. Padmanabhan, V. Subramanian, U. Sarkar, B. Maiti, P. Chattaraj, Toxicity analysis of benzidine through chemical reactivity and selectivity profiles: a DFT approach, Internet Electronic J. Molecular Des. 2 (2003) 798–813.
[48] S. Deep, J.C. Ahluwalia, Interaction of bovine serum albumin with anionic surfactants, Phys. Chem. Chem. Phys. 3 (2001) 4583–4591.
[49] S. Sonu, S. Halder, S. Kumari, R. Aggrawal, V.K. Aswal, S.K. Saha, Study on interactions of cationic gemini surfactants with folded and unfolded bovine serum albumin: effect of spacer group of surfactants, J. Mol. Liq. 243 (2017) 369–379.
[50] J.M. Khan, A. Ahmed, S.F. Alamery, M.A. Farah, T. Hussain, M.I. Khan, R.H. Khan, A. Malik, S. Fatima, P. Sen, Millimolar concentration of sodium dodecyl sulfate inhibit thermal aggregation in hen egg white lysozyme via increased α-helicity, Colloids Surf. 572 (2019) 167–173.